Heat-Flow-Based Analysis of Surface Crack Formation During the Start-Up of the Direct Chill Casting Process: Part II. Experimental Study of an AA5182 Rolling Ingot

J.B. WISKEL and S.L. COCKCROFT

The flow of heat during the start-up of the direct chill (DC) casting process has been studied with the aim of determining the factors that make this phase of the process prone to face crack generation. Measurements have been made on an AA5182 rolling ingot instrumented with embedded thermocouples placed at key locations in the vicinity of the ingot face near its base. The resulting temperature data have been input to a two-dimensional (2-D) inverse heat-transfer model, developed in part I of this two part study, in order to calculate heat flux *vs* surface temperature curves in the direct water impingement regime. The findings indicate that the flow of heat is influenced by changing surface morphology and water flow conditions during the start-up phase. A finite element based simulation of the cast start, employing the calculated flux/surface temperature relations, reveals that the ingot shell at the point of water contact reaches a maximum thickness early in the casting process. The location of this maximum was found to coincide with the position where surface cracks are routinely found to initiate. Further, this maximum was found to also coincide with position at which the rate of deflection of the base of the ingot ("butt-curl") begins to slow. Based on the heat-flow analysis, it is believed that the face cracks form due to an excessive shell thickness during transient start-up conditions and that their occurrence could be reduced by an optimal combination of water flow rate and casting speed during start-up.

I. INTRODUCTION

A critical part of any direct chill (DC) casting operation from the standpoint of crack formation and defect control is the start-up procedure. In many instances, failure to address problems stems from a lack of understanding and quantification of the heat-transfer phenomena occurring during this phase of the process. From the standpoint of heat transfer, the cast start-up is complicated, as it involves variations in both casting speed and water flow rate or other means of controlling heat transfer, such as pulsation of the water jet or injection of CO_2 gas into the water stream. In addition, the surface morphology of the ingot also undergoes a change from a relatively smooth lapped structure to a liquated, or textured, surface. Although direct water impingement is responsible for the removal of the majority of the sensible heat, and therefore is of paramount importance, it is also important to bear in mind the heat transport processes occurring in the mold, as they can have an influence on heat transfer below the mold.

In view of the preceding description, it is apparent that heat-transfer phenomena occurring at the start of the DC casting process do not lend themselves well to simulation in a laboratory setting. To this end, a two-dimensional (2-D) inverse heat-transfer method has been developed in part I of this study,[1] which is suitable for extricating heat fluxes from ingot temperature data collected during the start-up phase. Before proceeding with a description of the application of this method to an AA5182 rolling ingot, it is necessary to review the relevant literature, as the results of the inverse analysis must be analyzed in light of a mechanistic understanding of the factors that influence heat transfer to fluids.

II. BACKGROUND AND LITERATURE REVIEW

For the purpose of the discussion that follows, it is helpful to define a typical heat-flux curve correlating the rate of heat transport from the ingot to the DC water as a function of surface temperature. Such a curve is presented in Figure 1. The four heat-transfer regimes, in order of decreasing surface temperature, are (1) film boiling, (2) transition boiling, (3) nucleate boiling, and (4) natural or forced convection. Unfortunately, only a limited number of studies of this curve have been conducted on industrial casters. In one such study, Bakken and Bergstrom[2] analyzed the effect of casting speed on the magnitude and temperature of the peak flux (point A, Figure 1), as determined from cast-in thermocouples, for both billets and ingots. The temperature and magnitude of the maximum flux were found to depend on cooling water flow rate, spray geometry, and water temperature. Unfortunately, no specific details were given. The authors[2] also indicated that the magnitude of the maximum flux increased as casting speed was increased.

In a related study, Grandfield and Baker[3] have examined the effects of water flow rate, temperature, and CO_2 injection into the water stream on the surface temperature of 155-mm diameter, AA6063, extrusion billets. Qualitatively, it was observed that the surface temperature, at comparable

J.B. WISKEL, formerly with Alcan Research and Development, Kingston, ON, Canada, is Research Engineer, Department of Metals and Materials Engineering, The University of British Columbia. S.L. COCKCROFT, Assistant Professor, is with the Department of Metals and Materials Engineering, The University of British Columbia, Vancouver, BC, Canada, V6T 1Z4, is also associated with the Centre for Metallurgical Process Engineering.

Manuscript submitted March 27, 1995.

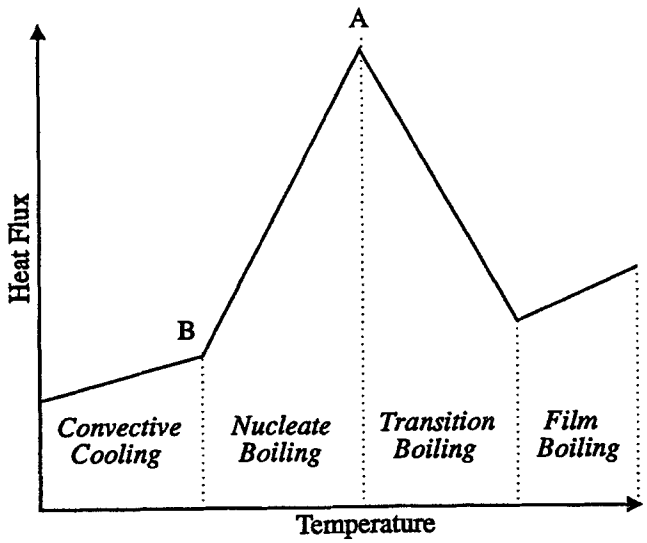

Fig. 1—Schematic of an idealized heat flux *vs* surface temperature curve for water cooling.

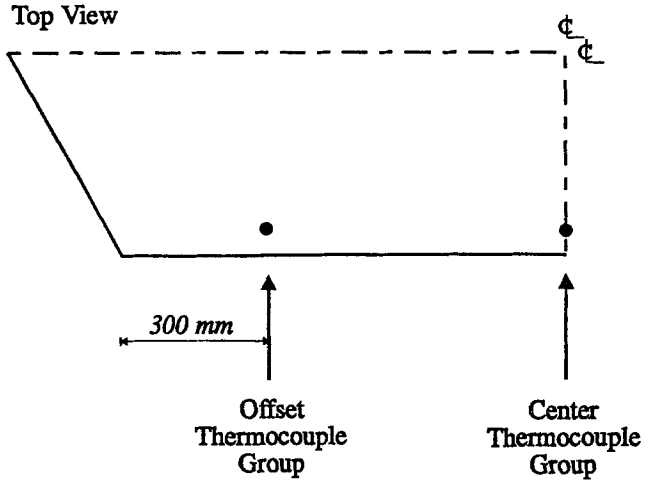

Fig. 2—Schematic of the transverse of an ingot quarter showing the placement of thermocouple groups.

distances below the mold, decreased with increasing water flow. Water temperature within the range of 20 °C to 35 °C was found to have only a negligible effect on the evolution of surface temperature, whereas the introduction of CO_2 in the water stream was found to have a significant effect. Similarly, Prasso *et al.*[4] observed a change in the near-surface isotherms in electromagnetic casting consistent with an increase in heat extraction as the water flow rate was increased from 208 to 265 L/m.

Taking a more mechanistic view, the transition boiling regime combines characteristics of both film and nucleate boiling, as it involves intermittent vapor film heat transfer and transient direct water contact (the proportion of the latter increasing with decreasing surface temperature). The amount of direct fluid/surface contact predominantly governs the magnitude of heat flux at a particular surface temperature.[5] Fundamental studies on heat transfer to fluids within this regime indicate an increase in the amount of heat extracted at any temperature with increasing cooling fluid mass flow rate[6,7,8] or velocity,[9] a shift in the position of maximum heat flux to lower temperatures with increasing surface roughness,[5,9–11] and an increase in the overall magnitude of the heat flux as the amount of subcooling increases[5,12] (amount by which the fluid is below its boiling temperature). In the studies on surface morphology, the magnitude of the peak flux was reported to either remain equal,[10] increase,[9,10] or decrease[11] in response to increasing surface roughness. The degree of subcooling was also observed to influence the shape of the transition flux curve.[6,12] In these studies on water temperature, the greatest effect on the transition curve was observed at low subcooling values.

At the peak heat flux (point A), the mechanism of heat transfer shifts from transition cooling to nucleate boiling, where heat is extracted by the generation and subsequent detachment of vapor bubbles from the surface.[11] Fundamental studies of this cooling regime indicate that the slope of the nucleate boiling portion of the curve is not appreciably influenced by cooling fluid flow[6,7,9] but is affected by surface roughness. For example, under conditions of pool boiling, increasing surface roughness was found to increase the slope of the nucleate boiling curve substantially[9,11] (*i.e.*, increasing heat extraction).

Finally, at surface temperatures below the boiling point of water (point B in Figure 1), heat is extracted by forced convection. Equations describing this type of heat transfer have been well developed.[9,13] Water flow rate is considered a dominate factor.[13] By increasing fluid flow, the heat extracted by the water at a particular surface temperature is increased.

In summary, the results of a review of the literature including more fundamental studies of fluid-based heat transfer provide an adequate and necessary foundation for interpretation of the results of an inverse heat-flow analysis of the DC water region of the DC casting process. They confirm that heat transport can be influenced by a number of the factors varying at the start of the casting process, including water flow rate/velocity, ingot withdrawal rate, ingot surface morphology, and surface temperature.

III. EXPERIMENTAL PROCEDURE

For the reasons outlined in Section I, it was deemed necessary to use thermal measurements acquired from a real casting system as a basis for an investigation of the DC water heat transfer. To this end, a series of thermocouples were embedded, or cast into, a production size (of nominal cross section 800 × 1680 mm) sheet ingot of alloy AA5182. A total of two casts were conducted at the Kaiser Aluminum Center for Technology research facility located in Pleasanton, CA. In addition to temperature data, ingot displacement was also measured dynamically using sensors located at the midpoint of the narrow face of each cast. The experimental procedure and apparatus are described in detail elsewhere.[14]

In total, two groups of thermocouples were cast into the ingot: one located at the center of the broad face and the other at a position offset 300 mm from the corner along this same broad face, as shown schematically in Figure 2. Each group consisted of three pairs of thermocouples. The pairs were positioned approximately 50, 150, and 250 mm from the ingot rim, as illustrated in Figure 3. In Figure 3,

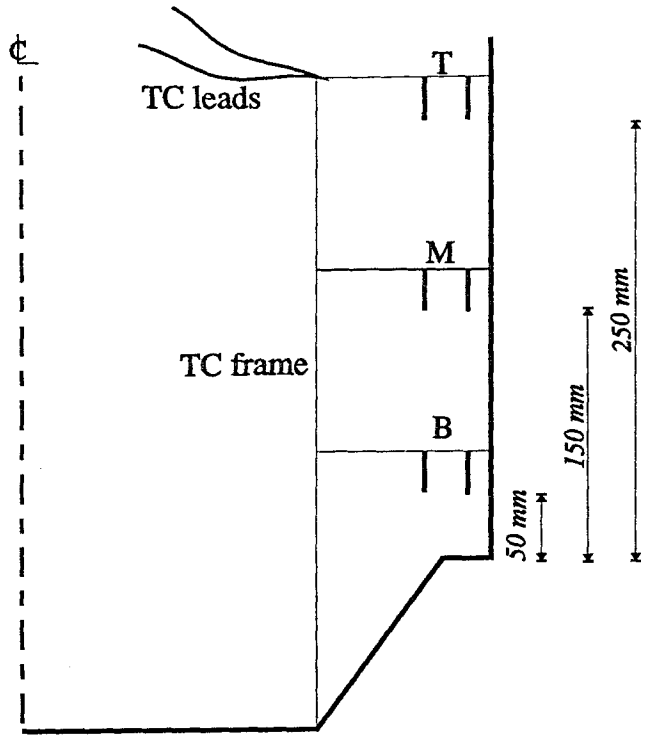

Fig. 3—Longitudinal cross section of an ingot showing the approximate axial positions of the thermocouple pairs in each group.

the designation B corresponds to the lower pair, M, to the middle pair, and T, to the upper pair. Each pair was comprised of one thermocouple located approximately 8 mm below the ingot surface, TC1, and one approximately 25 mm below the surface, TC2. The locations were chosen, first, to encompass the entire start-up region of the ingot and, second, to ensure that the flow of heat in the vicinity of the thermocouples would occur predominately in a plane oriented perpendicular to the broad face of the ingot and parallel to the withdrawal (axial) direction.[1] Following casting, the sections of ingot containing the thermocouples were extracted and machined to determine the location of the thermocouple leads.

As described in part 1,[1] the inverse heat-transfer analysis is based entirely on the thermal response of the near-surface thermocouple, TC1, whereas the temperatures from the deeper thermocouple, TC2, are used only for verification purposes. As a consequence, thermocouple pairs in which the response of the near-surface thermocouple was impaired, either due to a lack of physical entrainment or to electronic malfunctions, were not considered in the inverse analysis. The thermocouples that were deemed to have performed adequately are listed in Table I. Included in the table are the process conditions and surface morphology experienced by the thermocouple pair during the initial stages of direct water contact. Also included in Table I are the measured distances of each thermocouple from the surface, as determined from the postcast autopsy of the ingots.

Prior to the inverse analysis, a Savitzky–Golay[15] smoothing technique was applied to all of the TC1 temperature values in order to remove any random noise (this was found necessary in achieving a stable inverse solution). This technique employs a least-squares fit at a single temperature based on a fixed number of temperatures above and below this data point. For the purposes of this work, a quadratic function was used as the local regression equation. Typical thermocouple data before and after smoothing are presented for comparison in Figure 4. As can be seen, the trend in the data is unaffected and only the localized fluctuations in temperature have been minimized.

IV. RESULTS AND DISCUSSION

The thermocouple data from the casting trials have been analyzed with the inverse heat-transfer model according to the methodology outlined in part 1.[1] All the parameters input to the finite element method (FEM) conduction engine, including material properties, boundary conditions, initial conditions, and model control variables, are identical to those presented in Table I,[1] with the exception of the ingot withdrawal rate. The ingot withdrawal rates used are those taken from the actual casting and are presented in Table I for each thermocouple pair. The parameters pertaining to the inverse model employed in the analysis are identical to those presented in Table II.[1]

The basic formulation of the inverse model and code has been verified in part I[1] by analyzing hypothetical thermocouple data obtained from a model subject to a known heat flux profile. Before commencing with a discussion of the results of the inverse analysis of the industrial thermocouple data, it is important to verify the ability of the model to deal with real industrial data and to assess any errors that might have arisen.

A. *Verification and Error Assessment*

1. *Verification*

To begin, the inverse analysis must first predict correctly the temperature distribution in the casting in order to evaluate the temperature gradient at the ingot surface and, subsequently, the heat flux. To verify this aspect of the inverse calculation, the temperatures predicted by the inverse model can be compared with the measured temperatures. The results of one such comparison are presented in Figure 5. The plot contains a comparison for both thermocouples TC1 and TC2 that make up a typical cast-in pair. Refering to Table I, this particular data set was obtained in the second of the two castings from the top group located at the center of the broad face. As indicated previously, only the data from the thermocouple located closest to the surface are input to the inverse analysis; thus, the second thermocouple provides a means of independently assessing the inverse analysis. As can be seen, the results indicate good quantitative agreement for the thermocouple located nearest the ingot surface, TC1, and reasonable qualitative agreement for the second thermocouple located at greater depth, TC2. Overall, the comparison suggests that the inverse model has converged to a reasonable approximation of the 2-D temperature distribution in the vicinity of the ingot surface.

Another important aspect of the inverse analysis is that it must also correctly predict rates of change in temperature in order to determine the axial distribution of heat flux. To this end, a comparison has been made between the predicted and measured rates of change in temperature, or cooling rate, at the location of TC1. The results of this comparison are presented in Figure 6, which depicts the rate of change in temperature as a function of time or,

Table I. Placement of Thermocouples Used in Inverse Calculations

Thermocouple Pair	Cast Number	Cast Velocity (mm/s)	Water Flow (L/s/m)	Surface Morphology	Thermocouple Position (mm) TC1	TC2
Center–B	1	0.77 to 0.899	1.97	lapped	8.0	22.8
Center–T	1	0.899	3.33	exudated	12.5	28.5
Offset–M	1	0.899	1.97 to 3.33	transition	8.0	22.0
Offset–T	1	0.899	3.33	exudated	9.0	25.0
Center–B	2	0.77 to 0.899	1.97	lapped	9.0	20.0
Center–T	2	0.899	3.33	exudated	9.0	25.0
Offset–T	2	0.899	3.33	exudated	8.0	25.5

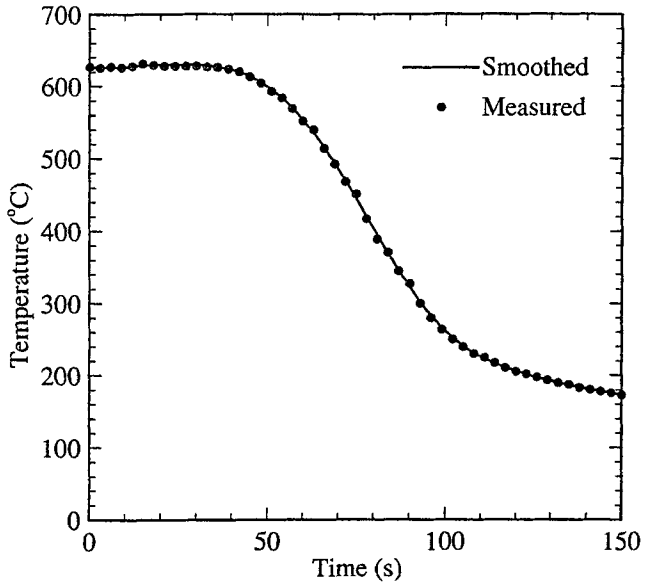

Fig. 4—Comparison of the measured TC1 temperatures at a cast 2:center-T thermocouple pair with smoothed TC1 data.

equivalently, position below the meniscus. The bottom of the mold has been identified on the graph to aid interpretation. As can be seen, these results indicate good agreement, particularly in the advanced cooling regime prior to water contact. At times greater than the peak cooling rate, the model predicted cooling rate slightly lags the measured value by up to 5 seconds or 4.5 mm, given a nominal casting speed of 0.899 mm/s.

Having achieved a measure of confidence in the model, it is now possible to shift focus to the predicted heat fluxes. The results of the inverse analysis proper are presented in Figure 7, which shows the surface heat flux attained after 12 seconds inverse analysis simulation time as a function of ingot surface temperature (12 seconds was found to be adequate for convergence of the inverse solution[1]). On close inspection, there are a several features of this plot which attest to its correctness. First, there is a clearly identifiable change in slope in the curve at around 100 °C, which delineates the transition from nucleate boiling to convective cooling; and second, the basic shape is similar to that of the idealized curve shown in Figure 1, which, in turn, is based on curves presented elsewhere.[2] The various regimes in order of decreasing temperature are approximately as follows: transition boiling, 525 °C to 134 °C; nucleate boiling, 134 °C to 100 °C; and convective cooling, below 100 °C. It should be noted that the calculated peak flux of 2.64 MW/m² is lower than that predicted by Bakken and Bergstrom,[2] which ranged from 4.0 to 5.6 MW/m², for a 1600 × 600 ingot. The reason for this difference is difficult to assess but may be related to differences in water flow rate, surface morphology, water quality, and alloy thermal diffusivity. To assess the influence of altering the thermal diffusivity of the alloy, the thermal conductivity used in the inverse analysis has been altered by ±10 pct over the published value (Table I).[1] As can be seen from the results presented in Figure 8, the heat flux is sensitive to thermal conductivity, particularly in the region of the peak. Increasing the thermal conductivity by 10 pct increases the peak flux from 2.64 to 2.82 MW/m².

Table II. Modified TC1 Locations

Thermocouple Pair	Corrected Distance from Surface (mm)	Adjustment (mm)
Cast 1: Offset–M	7.7	−0.3
Cast 1: Offset–T	9.7	0.7
Cast 1: Center–B	9.0	1.0
Cast 2: Offset–T	7.6	−0.4
Cast 2: Center–B	8.7	−0.3
Cast 2: Center–T	8.9	−0.1

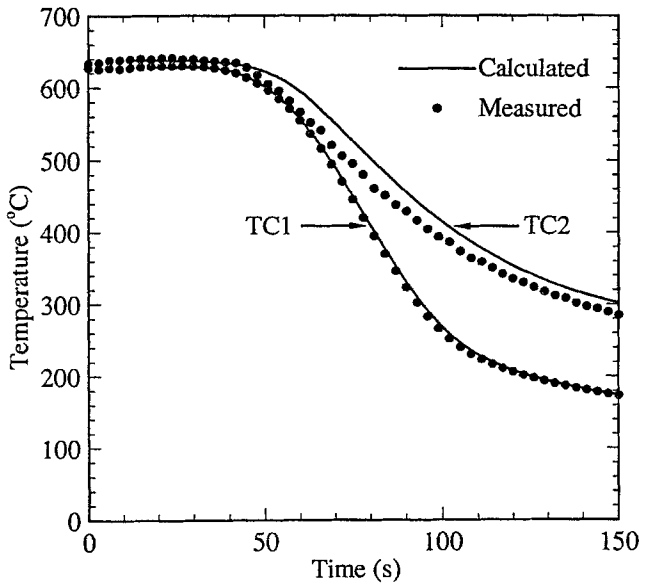

Fig. 5—Comparison of the measured temperatures at TC1 and TC2 at a cast 2:center-T thermocouple pair with the predicted values from inverse analysis.

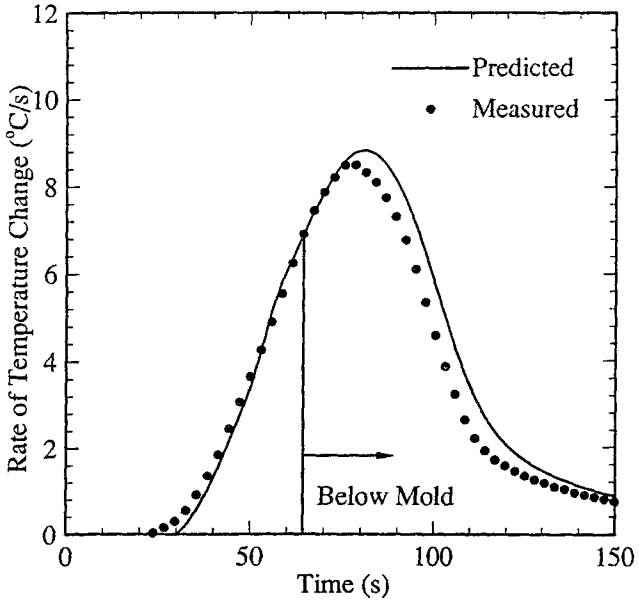

Fig. 6—Comparison of the measured rate of temperature change for TC1 at a cast 2:center-T thermocouple pair with the predicted value from inverse analysis.

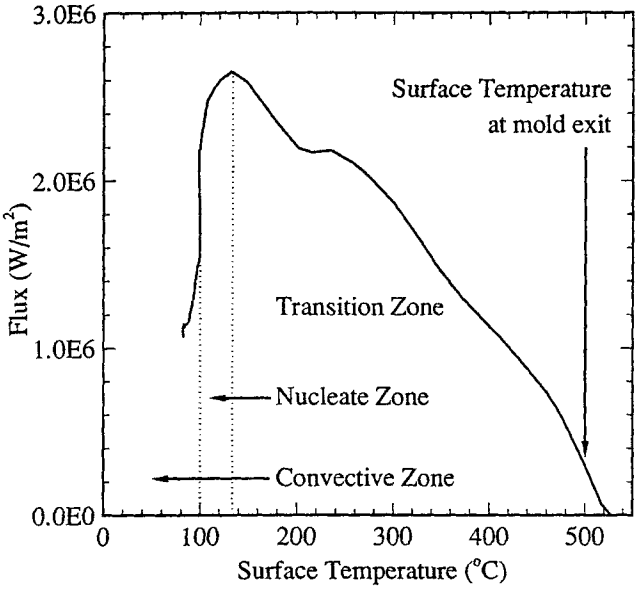

Fig. 7—Predicted heat flux *vs* surface temperature curve using data from TC1 at a cast 2:center-T thermocouple pair.

2. *Error assessment*

Although each of the castings was autopsied to determine the location of the embedded thermocouples, it is reasonable to assume some error in this measurement associated with both the physical width of the thermocouple and the nonuniformity of the ingot surface. In order to assess the effect of this uncertainty on the calculated heat flux profile, the location of TC1 has been varied by ±0.5 mm within the inverse analysis model. The results for TC1 depths of 8.5, 9.0, and 9.5 mm below the surface are presented in Figure 9. As can be seen from this figure, there are a number of features of the plot that are sensitive to thermocouple position, including the magnitude and temperature of the peak heat flux and the temperature of the transition from

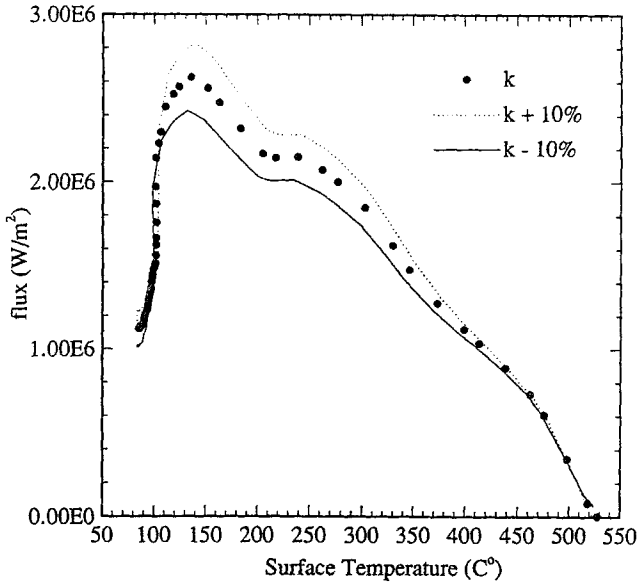

Fig. 8—Comparison of the calculated heat flux *vs* surface temperature curves for a ±10 pct change in thermal conductivity.

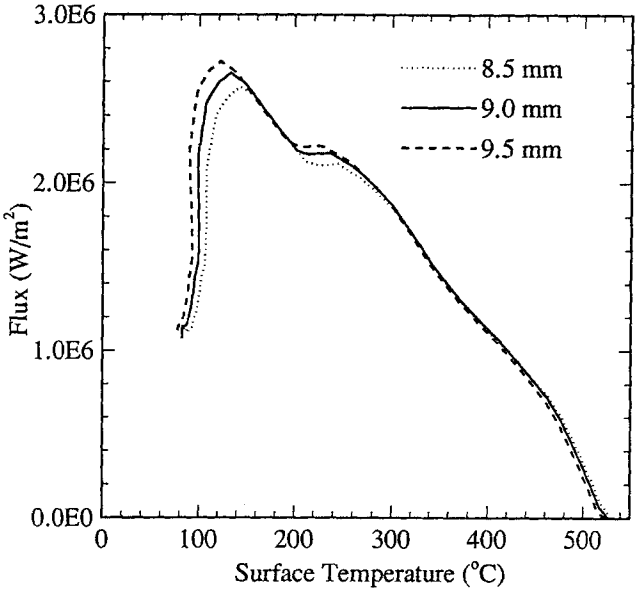

Fig. 9—Comparison of the calculated heat flux *vs* surface temperature curves for TC1 at 8.5, 9.0, and 9.5 mm using a cast 2:center-T thermocouple data.

nucleate to convective cooling. For example, varying the position from 8.5 to 9.5 mm is observed to result in a decrease in the temperature of the peak flux from 142 °C to 122 °C, an increase in the peak flux from 2.57 to 2.72 MW/m², and a decrease in the nucleate to convective transition temperature from 105 °C to 91 °C.

In summary, based on the results of the verification and error assessment, it is apparent that the inverse model is able to analyze industrial data with only one major concern, that of precisely determing the position of the embedded thermocouple (under the assumption that the thermophysical data input to the model is correct). Fortunately, the transition from nucleate boiling to convective cooling, which occurs at the boiling point of water (100 °C), can be used to "fine tune" the position of the TC1 thermocouple. This

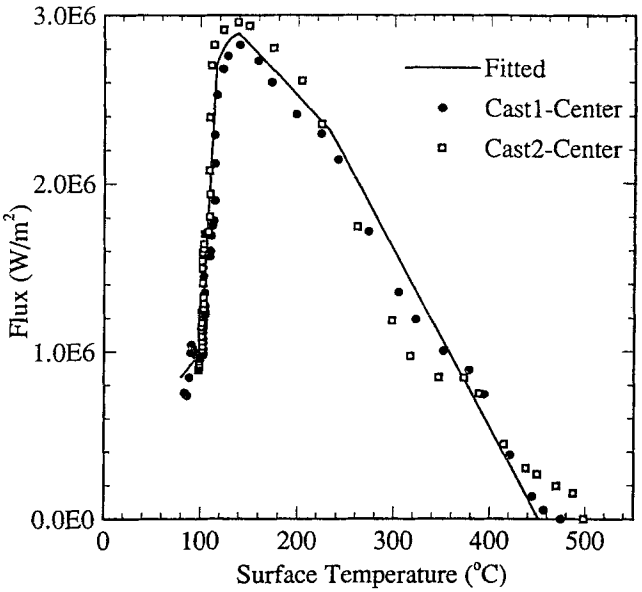

Fig. 10—Graph showing the calculated heat flux *vs* surface temperature curves for the B thermocouple pair and best-fit line.

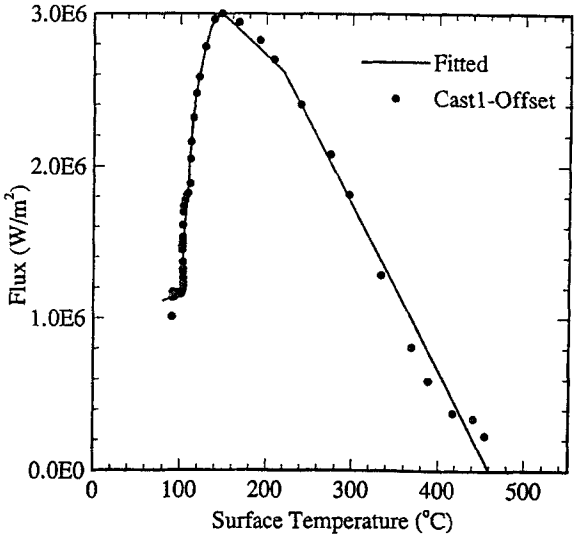

Fig. 11—Graph showing the calculated heat flux *vs* surface temperature curve for the M thermocouple pair and best-fit line.

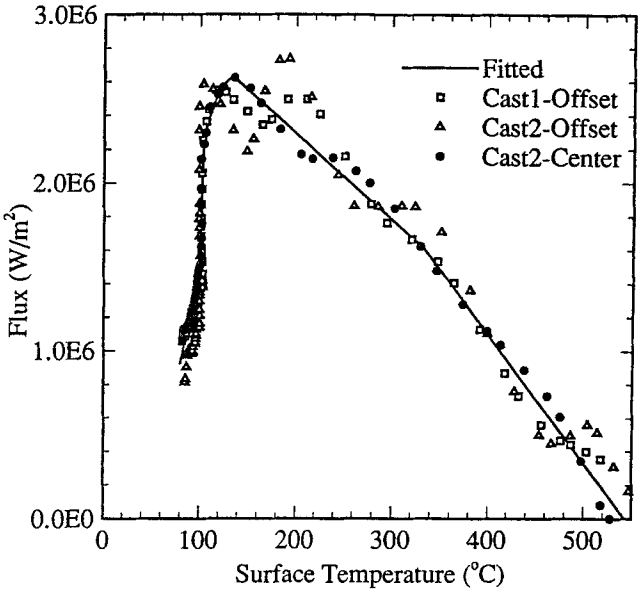

Fig. 12—Graph showing the calculated heat flux *vs* surface temperature curve for the T thermocouple pair and best-fit line.

has been done in all of the subsequent analyses. The resulting changes to all of the thermocouple postions have been summarized and are presented in Table II. It should be noted that in one instance, it was not possible to fit the thermocouple data to the nucleate boiling/convective cooling transition with a reasonable adjustment to the thermocouple depth. Close inspection of the original TC data revealed that this could be attributed to anomalous behavior in the rapid cooling portion of the temperature *vs* time curve, which impacted on the subsequent evolution of heat transfer predicted by the inverse model. In view of this, the data from the analysis of this thermocouple were subsequently removed from the investigation.

B. *Analysis of the Casting Process*

The results of the analysis of the remaining thermocouple data have been collated on the basis of vertical position in the casting (*e.g.*, bottom (B), middle (M), and top (T)) in an attempt to delineate the effect of changes in the casting parameters and ingot surface morphology on heat transfer. The results are presented in Figures 10 through 12. To help quantify the results, best-fit lines have been drawn through each of the various cooling regimes (*e.g.*, transitional boiling, nucleate boiling, and convective cooling). In Sections 1 through 3, the results are discussed in light of the mechanisms that influence heat transfer to fluids.

1. *Transitional cooling*

As seen in Figures 10 through 12, it proved necessary to employ two lines to represent the relationship between heat flux and ingot surface temperature in the transitional boiling regime. This result is somewhat unexpected in that, based on more fundamental studies,[5–11] one line should suffice. Mechanistically, it is reasonable to expect that the transition boiling behavior, which combines aspects of both film and nucleate boiling, could take time to develop and thus would in effect go through an initial transient before reaching heat fluxes characteristic of the surface temperature. Further, the behavior in the initial transient region would be dependent on the surface temperature at first water contact.

To determine any differences in the transition cooling regime that may arise due to changing process parameters, a comparison has been made between the best-fit lines to calculated cooling curves for the bottom (B), middle (M), and top (T), as shown in Figure 13. The most striking difference between the flow of heat in the bottom zone (lapped surface morphology, low water flow rate, and increasing casting speed) and that in the top zone (liquated surface morphology, high water flow rate, and high casting speed) is that the bottom zone exhibits a higher maximum flux than the top zone. At a glance, this is in contrast to what would be expected. However, it needs to be pointed out that the ingot surface has undergone a change from being lapped, or smooth, for the bottom thermocouple to being

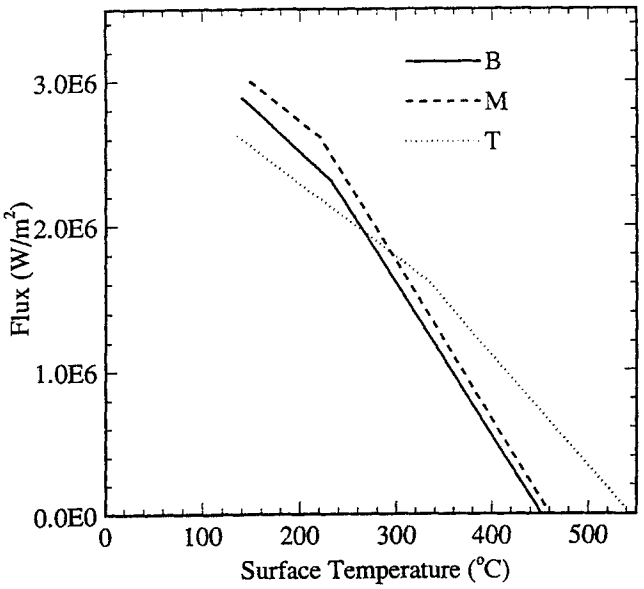

Fig. 13—Comparison of the best-fit curves of the transition regime for B, M, and T thermocouple pairs.

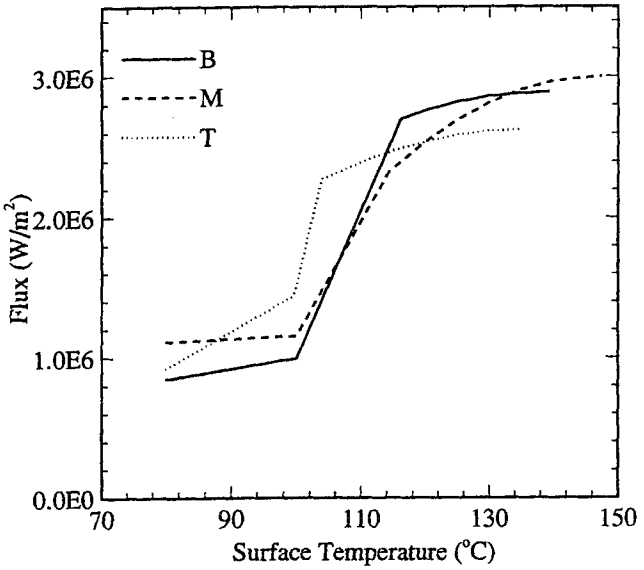

Fig. 14—Comparison of the best-fit curves of nucleate and convective regimes for B, M, and T thermocouple pairs.

liquated, or rough, for the top thermocouple. Based on a review of the relevant literature, it is possible that the effects of these two differences could offset one another. Hence, it would appear that in this instance, the increased surface roughness may be counteracting the influence of increased water flow, leading to a net drop in peak heat transfer. In addition, it is also worth noting that the rate of change of flux with surface temperature in the transient portion is higher for the bottom zone compared with that for the top zone. Presumably, surface roughness or water flow rate also plays a role in the development of transient, transition boiling heat transfer.

2. *Nucleate boiling*

The results of a comparison between the correlations for the bottom (B), middle (M), and top (T) zones for the nucleate boiling regime are presented in Figure 14. The results indicate that the top zone nucleate boiling line is shifted to lower temperatures relative to the curves based on data from the bottom and middle of the ingot. Mechanistically, a rougher surface would allow easier bubble nucleation, thus sustaining a more vigorous boiling (higher flux) to lower surface temperatures. A discernable difference also exists between the flux at which the transition from nucleate boiling to convective cooling occurs. At high water flow rate and rough surface (top zone), the transition occurs at 1.5×10^6 W/m^2, whereas for low water flow rate and smooth surface (bottom zone), the transition occurs at approximately 1.0×10^6 W/m^2. These results are consistent with other studies that have shown the transition heat flow to be proportional to water flow rate.[9,13]

3. *Effect of cooling water temperature*

Finally, a comparison of the cooling curves from the same locations in the two castings has been made in order to assess the influence of water temperature. The B zone thermocouple pair results, shown in Figure 10, indicate that the peak flux was slightly greater for the cast 2 (T_{water} = 19.4 °C) *vs* the colder cast 1 (T_{water} = 8.8 °C). This trend is opposite to what would be anticipated based on other investigations in the literature,[16,17] albeit these studies were conducted at much lower levels of subcooling.

In summary, combining the results of the inverse analysis, it is possible to develop two cooling curves to describe the heat flux variation with surface temperature during start-up; one applicable for conditions of low water flow and a lapped surface morphology (B zone, Figure 10) and the other for high water flow and an exudated surface (T zone, Figure 12). The trends observed are for the most part consistent with the literature and with a mechanistic understanding of the factors that influence the transfer of heat to fluids. The one notable exception is with respect to the influence of water temperature.

C. *2-D Simulation of Heat Transfer during Start-up and Investigation of Face Crack Initiation*

Having completed the inverse heat-transfer analysis of the thermocouple data, it is now possible to use the cooling curves to conduct a simulation of the start-up phase of the casting process. The purpose of the simulation is to examine the thermal behavior during this period with a view of trying to understand what makes this phase of the process particularly prone to face crack formation.

1. *Mathematical model*

The simulation was conducted employing a finite element based heat-transfer model, as described in detail elsewhere.[14] The analysis was 2-D and accounted for the change in geometry at the base of the ingot and for heat transfer to the mold, to the DC water, and to the bottom or starting block.[14] The DC boundary conditions are defined by the B cooling curve (Figure 10) for the first 180 mm of platform drop and by the T cooling curve for the remainder of the cast. The mold and bottom heat-transfer coefficients accounted for both direct contact and air gap cooling consistent with the surface morphologies observed.

The results of the finite element analysis are presented in Figure 15 in which the measured temperatures at the bottom, middle, and top for the center thermocouple group, in cast 2, are compared with the FEM predicted values. To

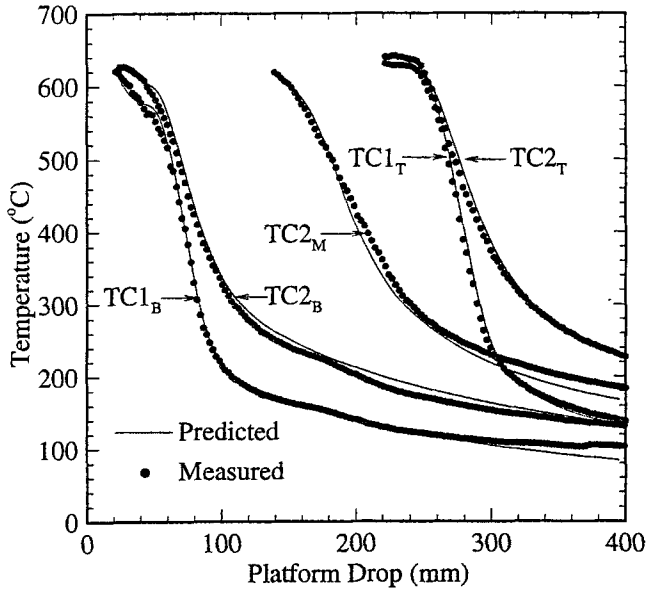

Fig. 15—Comparison of the measured data from the cast 2:center thermocouple group with predicted temperatures from FEM simulation.

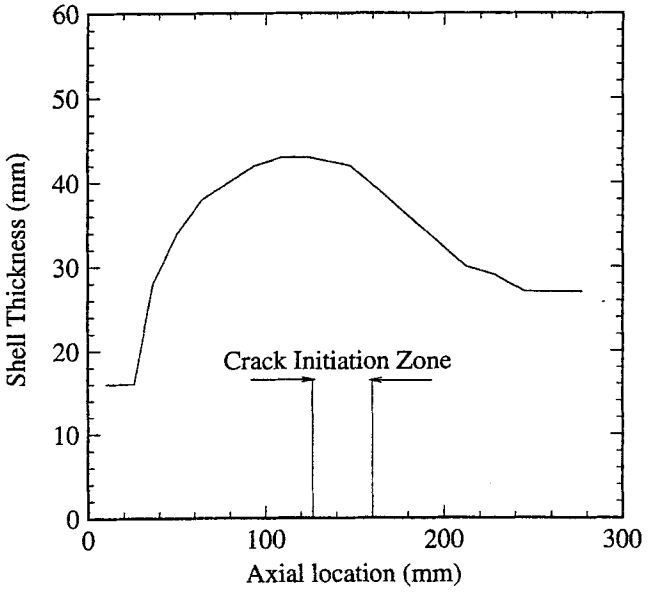

Fig. 16—Distance of the solidus (577 °C) isotherm from the surface at an axial location in the ingot parallel with the water contact line.

account for the final ingot deformation, an adjustment to the platform position of 7 mm was made to both the middle and top thermocouples to account for upward deformation occurring at the center of the long face. This value was measured following casting. No adjustment was made to the bottom thermocouple, as the amount of deformation that had occurred during its transit of the mold and the initial portions of the DC water cooling regimes was deemed negligible. Overall, as can be seen, application of the inverse conduction derived correlations achieves good agreement between the measured and predicted temperatures.

2. *Investigation of face crack initiation*

In the absence of surface tractions, thermally induced stresses arise from differential contraction on a local scale (*e.g.*, the cooler surface of the ingot has contracted more

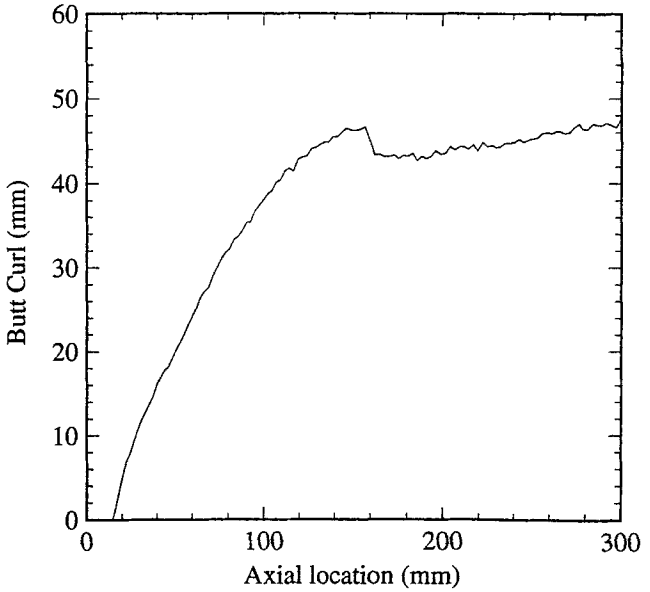

Fig. 17—Measured butt curl for cast 2 as a function of the axial location of the water contact line along the ingot surface.

than the hotter inner regions) and due to differential cooling on a global scale (*e.g.*, the corners and narrow face of the ingot cool more quickly than the broad face, generating a bending moment in the central region of the broad face). In the DC casting process, the tensile stresses that are responsible for the face cracking likely arise due the second mechanism, as the face cracks are generally limited to only the central region of the broad face (they do not arise over the entire face of the ingot in association with the high-temperature gradients observed below the line of water contact). Further, it is postulated that stresses generated by this mechanism will be enhanced by a thicker solid shell, as it will be less able to deform and "relax" the buildup of stress. Thus, insight into the cause of crack formation may be gained by examining the thickness of the solidified shell at the line of initial water contact.

Employing the temperature data from the FEM simulation, the thickness of the solidified shell (577 °C isotherm) at the point of water contact has been determined as a function of ingot withdrawal. The results are plotted in Figure 16, together with the locations on the ingot where face cracking is observed to initiate. As can be seen from the plot, the shell thickness reaches a maximum of approximately 43 mm at 115 mm before decreasing to the steady-state value of approximately 28 mm. Further, the zone of crack formation coincides closely with the position of maximum solidified shell thickness. The impact of the shell thickness at the point of water contact on the overall rigidity of the sump region is difficult to ascertain; however, some understanding can be gained from a plot of butt-curl *vs* ingot withdrawal (butt curl refers to the amount by which the base of the ingot is displaced from the bottom, or starter, block). The deformation arises due to thermally induced hoop stresses and is one of the mechanisms by which these stresses can be relaxed. Typically, the evolution of deformation has the form of Figure 17, which plots base displacement, as measured at the center of the narrow face *vs* axial position of the water contact point at the center of the long face. The results indicate that the rate of defor-

mation begins to slow at around 105 mm and eventually approaches zero at cast lengths greater than 300 mm. The reduction in the rate of deformation occurs, in part, due to a gradual increase in the structural rigidity of the base of the ingot. Comparing the results of Figure 16 with those of Figure 17, it is interesting to note that the point where the rate of butt curl begins to slow coincides closely with the point of maximum shell thickness and the beginning of the crack initiation zone. Presumably, the increase in shell thickness acts to augment the buildup in structural rigidity of the sump region of the ingot.

It follows from the preceding analysis that the face cracks arise due to a short-term, transient increase in the shell thickness which results in an increase in the constraining influence of the sump region of the ingot and an associated buildup in tensile thermal stresses. The proposed mechanisms will obviously have to be confirmed with thermal stress analysis. However, if correct, the propensity to form these cracks could be reduced by simply lowering the flow of water or increasing the casting speed in the stages leading up to the buildup of the maximum shell thickness. These parameters could be controlled so as to maintain a continuous and gradual increase in the shell thickness until the steady-state value is reached, thereby reducing the propensity for face cracks to occur.

V. CONCLUSIONS

The general inverse heat-transfer technique described in part I[1] has been employed to examine the flow of heat during the start-up of a full size rolling ingot. The results of the inverse analysis have been verified, first, by comparing the temperature, and rate of change of temperature, predicted by the inverse model with measured values and, second, by comparing the calculated flux *vs* surface temperature curves with similar curves presented in the literature.

The results of the inverse analysis indicate that the heat-flow conditions vary significantly during the start-up phase of the DC casting process. The most striking difference between the flow of heat in the bottom zone (lapped surface morphology, low water flow rate, and increasing casting speed) and the top zone (liquated surface morphology, high water flow rate, and high casting speed) is that the bottom zone exhibits a higher maximum flux than the top zone. The rationale for this behavior is that the effect of increased surface roughness (lapped to liquated) dominates the effect of increasing the flow of water. A second finding is that the top zone nucleate boiling line is shifted to lower temperatures relative to the curves based on data from the bottom and middle of the ingot. This result has been attributed to the effect of changing surface morphology and is consistent with data presented in the literature. Based on the results of the inverse analysis, two cooling curves have been developed to describe the heat flux variation with surface temperature during start-up: one applicable for conditions of low water flow and a lapped surface morphology and the other for high water flow and an exudated surface.

Using the correlations developed from the inverse heat-transfer analysis, a simulation of the start-up phase of the casting process has been conducted. Based on the results of the heat-flow analysis, the thickness of the solidified shell (577 °C isotherm) at the point of water contact has been found to reach a maximum at approximately 115 mm of ingot drop. Further, the point of maximum shell thickness was found to coincide with the location of face crack initiation. It is believed that the added constraint imposed on thermal contraction by the thick solidified shell is sufficient to cause elevated tensile stresses responsible for face crack initiation. If correct, it follows that a better combination of water flow rate and ingot withdrawal rate, during the start-up phase, could be used to achieve a gradual increase in the shell thickness and thereby reduce the propensity to form face cracks.

REFERENCES

1. J.B. Wiskel and S.I. Cockcroft: *Metall. Mater. Trans. B*, 1995, vol. 26B, pp. 119-28.
2. J.A. Bakken and T. Bergstrom: *Light Metals 1986*, R.E. Miller, ed., TMS, Warrendale, PA, 1986, pp. 883-91.
3. J. Grandfield and P.W. Baker: *Proc. 3rd Int. Conf. of Solidification Processing*, Institute of Metals, North American Publishing Center, Brookfield, VT, 1987, pp. 260-63.
4. D.C. Prasso, J.W. Evans, and I.J. Wilson: *Light Metals 1994*, U. Mannweiler, ed., TMS, Warrendale, PA, 1986, pp. 871-77.
5. H. Auracher: *Heat Transfer 1990*, G. Hetsroni, ed., Hemisphere Publishing Corp., New York, NY, 1990, vol. I, pp. 69-90.
6. S.C. Cheng, W.W.L. Ng, and K.T. Heng: *Int. J. Heat Mass Transfer*, 1978, vol. 21, pp. 1385-92.
7. Chin Pan and K.T. Ma: *Proc. Eng. Found. Conf. Pool and External Flow Boiling*, ASME, Fairfield, NI, 1992, pp. 263-70.
8. X.C. Huang, P. Weber, and G. Bartsch: *Int. Comm. Heat Mass Transfer*, 1993, vol. 20, pp. 383-92.
9. F.M. White: *Heat and Mass Transfer*, Addison-Wesley Publishing Co., Reading, MA, 1991, pp. 561-64.
10. V.K. Dhir: *Heat Transfer 1990*, G. Hetsroni, ed., Hemisphere Publishing Corp., New York, NY, 1990, vol. I, pp. 129-55.
11. M. Shoji, L.C. Witte, S. Yokoya, and M. Ohshima: *Proc. 9th Int. Heat Transfer Conf.*, Jerusalem, Israel, Hemisphere Publishing Corporation, New York, N.Y., 1990, vol. 2, pp. 135-40.
12. M. Bamberger and B. Prinz: *Mater. Sci. Technol.*, 1986, vol. 2, pp. 410-15.
13. D.C. Weckman and P. Niessen: *Metall. Trans. B*, 1982, vol. 13B (12), pp. 593-602.
14. J.B. Wiskel: Ph.D. Thesis, The University of British Columbia, Vancouver, BC, Canada, 1995.
15. W.H. Press, S.A. Teukolsky, W.T. Vetterling, and B.P. Flannery: *Numerical Recipes in Fortran: The Art of Scientific Computing*, 2nd ed., Cambridge University Press, Cambridge, United Kingdom, 1992, pp. 644-47.
16. S.C. Cheng, W.W.L. Ng, and K.T. Heng: *Int. J. Heat Mass Transfer*, 1978, vol. 21, pp. 1385-92.
17. C.F. Ma, Y.P. Gan, Y.C. Tian, and D.H. Lei: *J. Thermal Sci.*, 1993, vol. 2 (1), pp. 32-49.